Chapter 21
Measurement of Skin Elasticity Using High Frequency Ultrasound Elastography with Intrinsic Deformation Induced by Arterial Pulsation

Ryo Nagaoka, Kazuto Kobayashi, and Yoshifumi Saijo

Abstract Mechanical property of the skin is one of the important factors for diagnosis of human skin diseases. In this paper, we proposed a novel method for estimation of shear wave velocity from deformation induced by an arterial pulsation. The induced deformation was measured by high frequency ultrasound. The elasticity of the in vivo human skin is evaluated based on the calculated parameters. P(VDF-TrFE) transducer with the central frequency of 100 MHz was used for imaging. The aperture diameter of the transducer was 2 mm, and the focal length was 4 mm. The repetition rate was 2,600 Hz. The sampling rate was 1 GS/s with 8 bit. The velocity induced by pulsation was measured by 1-D cross-correlation method at each depth. The shear wave velocity was estimated from the measured velocity. The shear wave velocity at the epidermis was 0.14 m/s, and the velocity at the dermis was 0.06 m/s. Because the stiffness of the skin was proportional to the shear wave velocity, the elasticity of the epidermis was higher than that of the dermis. These estimated elasticity well conformed to the histology of the skin and the past reports.

Keywords Elasticity • High frequency Ultrasound • Shear wave velocity • Skin

21.1 Introduction

Mechanical properties of human skin are the important factors not only in medicine field but also in cosmetic field. Especially, viscoelasticity of human skin is closely related to collagen and elastin of human skin. Also, it's considered that the

R. Nagaoka (✉) • Y. Saijo
Graduate School of Biomedical Engineering, Tohoku University, 2-1, Seiryo-machi, Aoba-ku, Sendai 980-8579, Japan
e-mail: ryo@ecei.tohoku.ac.jp

K. Kobayashi
Division of Research and Development, Honda Electronics Co., Ltd., Toyohashi 411-3193, Japan

K. Sasaki et al. (eds.), *Interface Oral Health Science 2014*,
DOI 10.1007/978-4-431-55192-8_21

viscoelasticity is linked to microstructures within the dermis, which are sebaceous glands, hair follicles, and capillary blood vessels. Flexibility and retractility of human skin may change with the changes in these combinations.

High frequency ultrasonography (HFUS) enables to achieve high-resolution measurement because the resolution is equal to one-half wavelength of ultrasound. An axial resolution of 20 μm is acquired at 75 MHz, and a penetration depth of 75 MHz ultrasound is about 2.0 mm at most. HFUS with a center frequency of 100 MHz is much suitable for in vivo measurement of human skin because it's possible to observe not only the microstructures but also whole area of human skin. The microstructures of the human skin have been observed by HFUS at the central frequency of 100 MHz [1]. The hair follicles were reported as hypo echoic and the dermis was reported as echo-rich. Also, the human skin was observed using spherical focused single-element transducer with a center frequency of 20 MHz, [2] and the elasticity of the skin was assessed by applying suction to the skin surface with a stepwise increase in vacuum [3]. Additionally, the nevus inside the dermis was observed by strain imaging. In our previous study [4], the human skin structures, especially the sebaceous glands deeper in dermis, were observed by three-dimensional ultrasound microscopy with a central frequency of 120 MHz. This study revealed that the sebaceous glands also act as a cushion of the skin in addition to their classical role of secreting sebum and some hormones [5]. Additionally, viscoelasticity of the skin was estimated from displacements measured by Cutometer (MPA580, Courage and Khazaka, Kȯln, Germany) and Voigt model [6].

Elastography is a common technique that estimates mechanical properties of the tissue. Especially, viscoelasticity is a key parameter for a diagnosis of cancer and fibrosis. There are several kinds of elastography: strain elastography [7–11], acoustic radiation force impulse (ARFI) imaging [12–17], shear wave elastography [18–22] and transient elastography [23, 24]. The difference among these techniques is difference of what induces the deformation inside tissues. Recently, passive elastography [25, 26] has been attracted attention. This passive elastography is based on Green's function retrieval and utilize periodic physical motions, which are induced by heartbeats, breathing and so on. In our research group, deformations inside in vivo skin due to arterial pulsation were measured by HFUS with 100 MHz, and the viscoelasticity of human skin was evaluated based on measured deformation itself.

Our goal is to develop high frequency ultrasound elastography using intrinsic deformation induced by pulsation to reveal the origin of the skin viscoelasticity. In this paper, we proposed a novel method for estimation of elasticity the arterial pulsation as an intrinsic deformation. The induced deformation is measured by high frequency ultrasound, and the velocity is calculated from the displacements at several points. The elasticity of the in vivo human skin is evaluated based on the calculated parameters.

21.2 Method

21.2.1 Data Acquisition Setup

Figure 21.1 shows a schematic of an experiment system. An electric impulse was generated by a high speed switching semiconductor. The start of the pulse was within 400 ps, the pulse width was 2 ns and the pulse voltage was 40 V. The frequency of the impulse covered up to 500 MHz. The electric impulse was used to excite a vinylidene fluoride and trifluoroethylene P(VDF-TrFE) transducer. The aperture diameter of the transducer was 2.0 mm, and the focal length was 4 mm. The central frequency was 100 MHz, the bandwidth (−6 dB) was 40–120 MHz, and the pulse repetition rate was 2,800 Hz. First, the transducer was mounted on the X-Y scanner with two linear servo motors that were controlled by X-Y scan controller connected to the serial port of the PC. The scan area was 2×2 mm with 100×100 pixels. Four pulse echo sequences with 4,096 sampling points along the depth z were averaged for each scan point in order to increase the S/N ratio. Consecutive 100 B-mode images were produced from the RF data by a conventional image processing algorithm of echography. Next, the measured positions were decided from the B-mode images. Figure 21.2 shows a schematic of an elasticity measurement. In this paper, a deformation induced by the pulsation was used as a source. With the position of the transducer fixed, the reflections from the skin in a forearm were received by the transducer and were introduced into a Windows-based personal computer (PC; Pentium 4, 3.40 GHz, 1 GB RAM, and 250 GB HDD) with a high-speed digitizer card (Acqiris DP 1400, Geneva, Switzerland). The sampling rate was 1 GS/s. The duration of the measurement was 2.5 s.

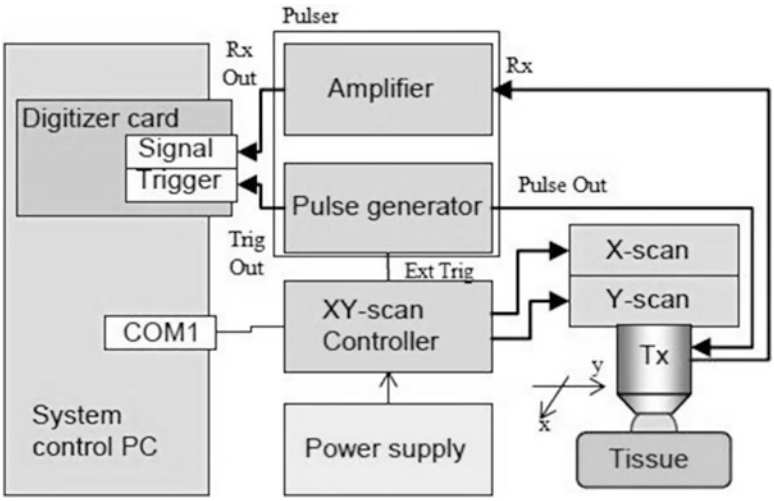

Fig. 21.1 Block diagram of 3D ultrasound microscope system

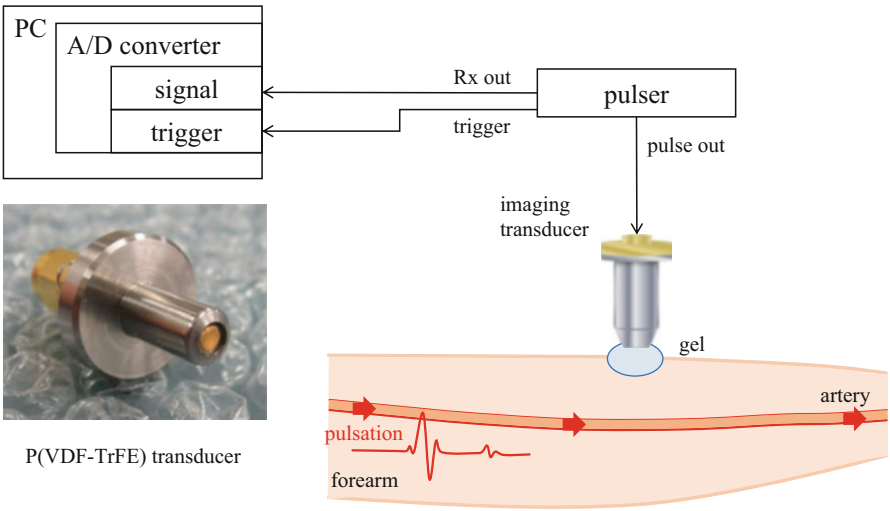

Fig. 21.2 Schematic of elasticity measurement

The received data were converted to M-mode images. Obtained RF signals of each scanning line was converted to B-mode image by a conventional image processing algorithm of echography.

21.2.2 Subject

Subject is one 24-year-old healthy male. A measurement area is skin in his forearm.

21.2.3 Velocity Measurement

The velocity induced by the pulsation was measured from the RF echo data of the fixed position by implementing a 1-D cross correlation method. RF signal of time t at depth z was defined as $\boldsymbol{r_t}(z)$. Analytical signal $\boldsymbol{g_t}(z)$ was obtained by applying the Hilbert transform to the RF signal $\boldsymbol{r_t}(z)$. Pulse waves with angular frequency $\boldsymbol{\omega_0 = 2\pi f_0}$ were transmitted at a time interval of $\boldsymbol{\Delta T}$. Analytical signal of time t and t + $\boldsymbol{\Delta T}$ at depth z can be modeled as

$$g_t(z) = u(z)exp\left\{-i\left(\omega_0 \frac{2f_s}{c_0} z - \theta_0\right)\right\}, \tag{21.1}$$

$$g_{t+\Delta T}(z) = u(z)exp\left[-i\left\{\omega_0 \frac{2f_s}{c_0}(z - z_\tau) - \theta_0\right\}\right], \tag{21.2}$$

where $\boldsymbol{u}(z)$ was the envelope of the analytical signal, $\boldsymbol{f_s}$ was the sampling frequency, $\boldsymbol{c}_0$ was the sound speed, $\boldsymbol{\theta}_0$ was the initial phase, and $\boldsymbol{z_\tau}$ was the true displacement induced by the pulsation. The complex cross-correlation function $\boldsymbol{\gamma(z_{lag})}$ at lag $\boldsymbol{z_{lag}}$ was defined as

$$\gamma(z_{lag}) = \frac{\sum_{z=-\frac{N}{2}}^{z=\frac{N}{2}} g_t^*(z) g_{t+\Delta T}(z + z_{lag})}{\left|\sum_{z=-\frac{N}{2}}^{z=\frac{N}{2}} g_t^*(z)\right| \left|\sum_{z=-\frac{N}{2}}^{z=\frac{N}{2}} g_{t+\Delta T}(z + z_{lag})\right|} \tag{21.3}$$

where N was 1-D cross correlation window of 256 pixels, corresponding to 195 μm depth window with 91 % overlap using hamming window. An index at maximum value of the real part of the Eq. (21.3) corresponded to the index of $\widehat{z}_{lag}$. In this paper, f_s was 1 GHz, and the temporal resolution was enough high to observe the deformation with HFUS of 100 MHz. Additionally, the received RF signal was up-sampled to 4 GHz before implementing the 1-D cross-correlation. Because of these reasons, the estimated displacement $\widehat{z}_{lag}$ was almost equal to the true displacement z_{lag}. The velocity, denoted by $v_{t+\Delta T/2}(z)$, of the skin in his forearm between the interval was given as follows:

$$v_{t+\Delta T/2}(z) = \frac{c_0 \widehat{z}_{lag}}{2f_s \Delta T}. \tag{21.4}$$

The acceleration was calculated from the measured velocity. The acceleration was calculated by differentiating the measured velocity as

$$a_t(z) = \frac{v_{t+\Delta T/2}(z) - v_{t-\Delta T/2}(z)}{\Delta T}. \tag{21.5}$$

21.2.4 Shear Wave Measurement

By comparing an acceleration at reference depth with an acceleration at interest depth, a velocity of shear wave propagating from an artery toward a skin surface can be calculated from a relationship between the depth and the arrival time of shear wave at the depth. The relationship φ(z) can be expressed as

$$\varphi(z) = \frac{\sum_{t=-\frac{N_\alpha}{2}}^{t=\frac{N_\alpha}{2}} a_t^*(z_0) \cdot a_t(z)}{\left|\sum_{t=-\frac{N_\alpha}{2}}^{t=\frac{N_\alpha}{2}} a_t^*(z_0)\right| \left|\sum_{t=-\frac{N_\alpha}{2}}^{t=\frac{N_\alpha}{2}} a_t(z)\right|}, \tag{21.6}$$

where N_α was an estimation window of 50 pixels, corresponding to a 50 ms time. A hamming window was used for the estimation. A variable z_0 was a reference

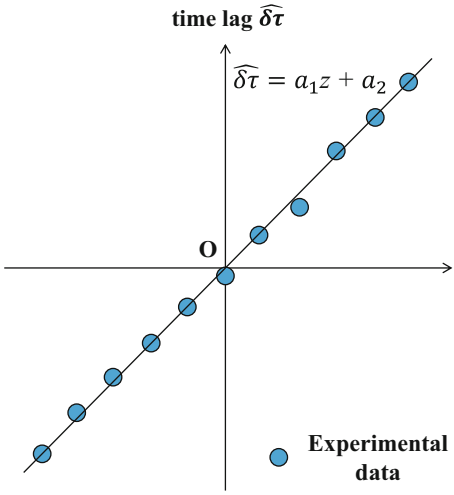

Fig. 21.3 Relationship between depth and time lag. *Dots*: experiments data, and *line*: regression line calculated by least square method

depth, and a variable z was an interest depth. A time lag between the reference depth and the interest depth was expressed as follows:

$$\delta\tau(z) = \frac{\varphi(z)}{2\pi f_c} \tag{21.7}$$

The center frequency f_c was obtained from the power spectrum calculated by applying the Fourier transform to the acceleration signals. Figure 21.3 shows the relationship between the depth z and the time lag. A regression line can be obtained by applying the least square method to the relationship. A slope a_1 of the regression line can be obtained by minimizing a least mean square error e as follows:

$$\mathrm{e} = \sum_{z=0}^{z=Z_N} |\delta\tau(z) - (a_1 z + a_2)|^2 \tag{21.8}$$

A variable Z_N is a total number of the region of interest. The velocity C_s of shear wave was given by dividing the depth distance Δz by the estimated slope value $\widehat{a}_1$:

$$C_s = \frac{\Delta z}{\widehat{a}_1} \tag{21.9}$$

21.3 Results

21.3.1 Measurement of Deformation

Figure 21.4 shows a B-mode image of the skin. In the B-mode image, an epidermis and a dermis were clearly distinguished. A scan line for an M-mode image was decided from the B-mode image (a red line). Figure 21.5 shows an M-mode image

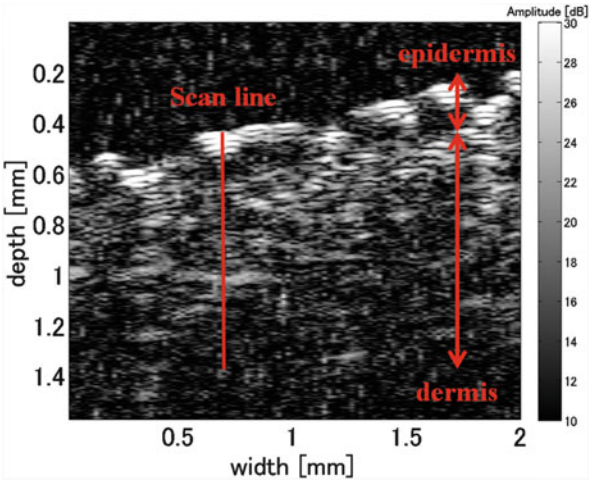

Fig. 21.4 B-mode image of human skin of forearm

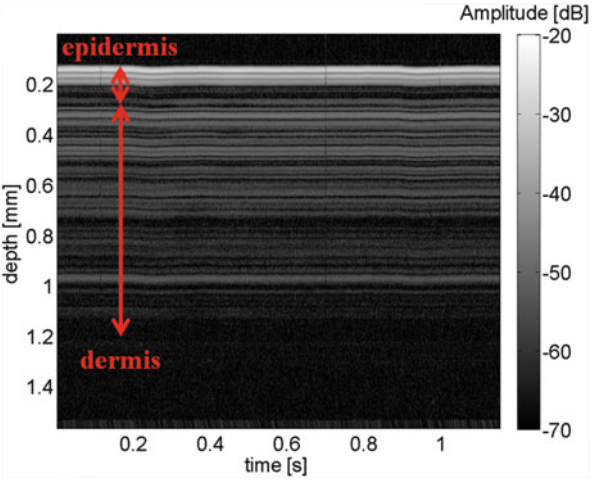

Fig. 21.5 M-mode image of scan line in human skin

of the scan line in the skin. In the M-mode image, each layer was slightly pulsating. Figure 21.6 shows a result of a velocity measurement. Figure 21.6a shows a velocity waveform, and Fig. 21.6b shows the velocity at each depth (surface, 0.20, 0.40, 0.60, and 0.80 mm). Figure 21.7 shows a result of an acceleration measurement. Figure 21.7a shows an acceleration waveform, and Fig. 21.7b shows the acceleration at each depth (surface, 0.20, 0.40, 0.60, and 0.80 mm).

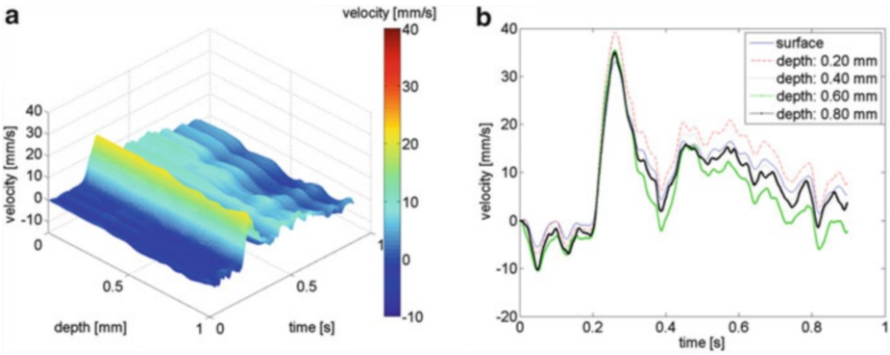

Fig. 21.6 Measured velocity of scan line; (**a**) velocity waveform, and (**b**) velocity at each depth (skin surface, 0.20, 0.40, 0.60, and 0.80 mm, respectively)

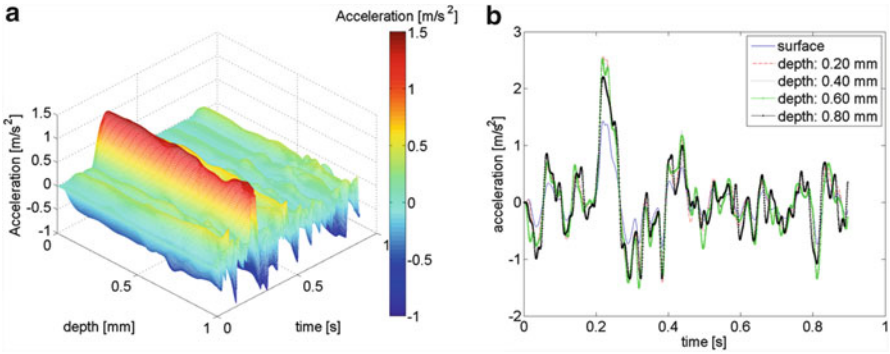

Fig. 21.7 Measured acceleration of scan line; (**a**) acceleration waveform, and (**b**) acceleration at each depth (skin surface, 0.20, 0.40, 0.60, and 0.80 mm, respectively)

21.3.2 Estimated Shear Wave Velocity

Figure 21.8 shows the acceleration waveform map. 3 regions of interest (ROI I, II, and III) were set in the M-mode image. ROI I corresponded to an area of the epidermis, ROI II corresponded to an area of border between the epidermis and dermis, and ROI III corresponded to an area of the dermis. Figure 21.9a shows a close-up image of ROI I, and Fig. 21.9b shows a relationship between time and depth with a regression line. In the region of the epidermis, the shear wave velocity was 0.14 m/s. Figure 21.10a shows a close-up image of ROI II, and Fig. 21.10b shows a relationship between time and depth with a regression line. In the region of the border, the shear wave velocity was 0.04 m/s. Figure 21.11a shows a close-up image of ROI II1, and Fig. 21.11b shows a relationship between time and depth with a regression line. In the region of the dermis, the shear wave velocity was 0.06 m/s.

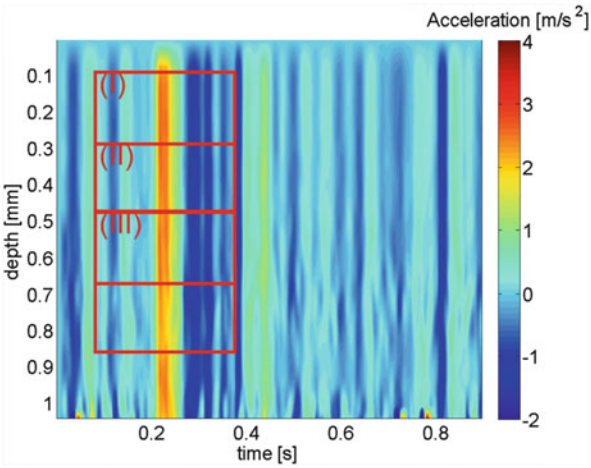

Fig. 21.8 Measured acceleration map. ROI I: area of epidermis, ROI II: area of border between epidermis and dermis, and ROI III: area of dermis

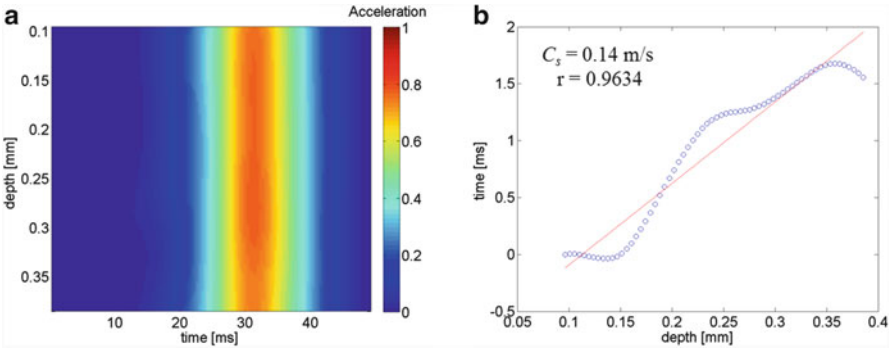

Fig. 21.9 (**a**) Close-up image of ROI I, and (**b**) relationship between time and depth with regression line

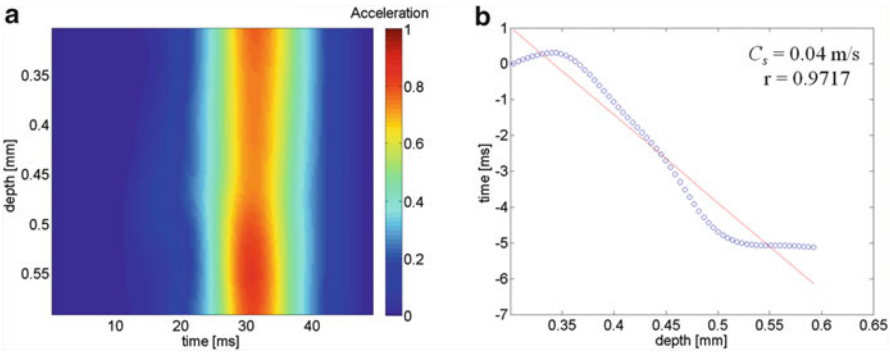

Fig. 21.10 (**a**) Close-up image of ROI II, and (**b**) relationship between time and depth with regression line

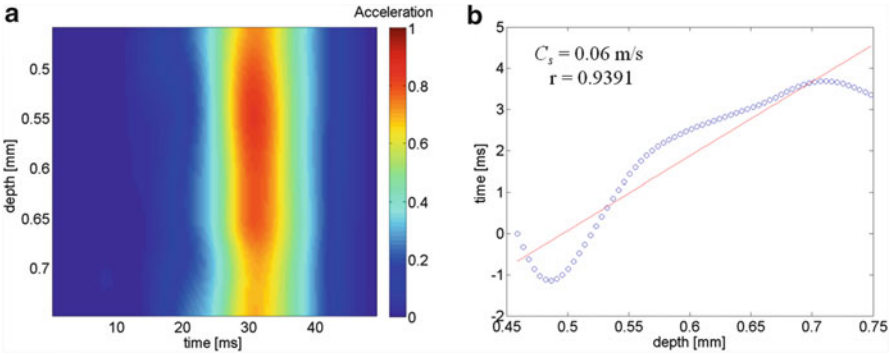

Fig. 21.11 (**a**) Close-up image of ROI III, and (**b**) relationship between time and depth with regression line

21.4 Discussion

The measured shear wave velocity of ROI I was higher than that of ROI II, and this results conformed to the past researches that the elasticity of the epidermis is higher than that of the dermis. Due to use of low frequency in analysis of acceleration, the measured shear wave velocity was lower.

21.5 Conclusion

The deformation induced by arterial pulsation were measured with high frequency ultrasound. The acceleration and the shear wave velocity were calculated from the measured velocity. These estimated parameters well conformed to the histology of the skin and the past reports. We believe this proposed method is very useful to evaluate the elasticity of the human skin.

References

1. Gammal SE, Gammal CE, Kaspar K, Pieck C, Altmeyer P, Vogt M, Ermert H. J Invest Dermatol. 1999;113:821.
2. Vogt M, Ermert H. IEEE Trans Ultrason Ferroelectr Freq Control. 2008;55:1975.
3. Vogt M, Ermert H. IEEE Trans Ultrason Ferroelectr Freq Control. 2005;52:375.
4. Kumagai K, Koike H, Kudo Y, Nagaoka R, Kubo K, Kobayashi K, Saijo Y. Proceedings of the conference of 33rd IEEE EMBC; 2011, p. 7199.

5. Kumagai K, Koike H, Nagaoka R, Sakai S, Kobayashi K, Saijo Y. Ultrasound Med Biol. 2012;38:1838.
6. Nagaoka R, Kobayashi K, Saijo Y. Proceedings of the conference of 35th IEEE EMBC; 2013, p. 1112.
7. Krouskop TA, Doughtery DR, Levinson SF. J Rehabil Res Dev. 1987;24:1.
8. Yamakoshi Y, Sato J, Sato T. IEEE Trans Ultrason Ferroelectr Freq Control. 1990;37:45.
9. Ophir J, Cespedes I, Ponnekanti H, Yazdi Y, Li X. Ultrason Imaging. 1991;13:111.
10. Shiina T, Doyley MM, Bamber JC. Proceedings of the IEEE ultrasonics symposium; 1996, p. 1331.
11. Yamakawa M, Shiina T. Jpn J Appl Phys. 2001;40:3872.
12. Nightingale K, Soo MS, Nightingale R, Trahey G. Ultrasound Med Biol. 2002;28:227.
13. Nightingale K, McAleavey S, Trahey GE. Ultrasound Med Biol. 2003;29:1715.
14. Bercoff J, Tanter M, Fink M. IEEE Trans Ultrason Ferroelectr Freq Control. 2004;51:396.
15. Chen S, Fatemi M, Greenleaf JF. J Acoust Soc Am. 2002;112:884.
16. Hasegawa H, Takahashi M, Nishio Y, Kanai H. J Appl Phys. 2006;45:4706.
17. Yamaguchi J, Hasegawa H, Kanai H. J Med Ultrasound. 2012;39:279.
18. Sandrin L, Tanter M, Catheline S, Fink M. IEEE Trans Ultrason Ferroelectr Freq Control. 2002;49:426.
19. Tanter M, Bercoff J, Sandrin L, Fink M. IEEE Trans Ultrason Ferroelectr Freq Control. 2002;49:1363.
20. Montaldo G, Tanter M, Bercoff J, Benech N, Fink M. IEEE Trans Ultrason Ferroelectr Freq Control. 2009;56:489.
21. Chen S, Fatemi M, Greenleaf JF. J Acoust Soc Am. 2004;115:2781.
22. Chen S, Urban MW, Pislaru C, Kinnick R, Zheng Y, Yao A, Greenleaf JF. IEEE Trans Ultrason Ferroelectr Freq Control. 2009;56:55.
23. Sandrin L, Tanter M, Gennisson JL, Catheline S, Fink M. IEEE Trans Ultrason Ferroelectr Freq Control. 2002;49:436.
24. Sandrin L, Fourquet B, Hasquenoph JM, Yon S, Fournier C, Mal F, Christidis C, Ziol M, Poulet B, Kazemi F, Beaugrand M, Palau R. Ultrasound Med Biol. 2003;29:1705.
25. Brum J, Benech N, Negreira C, Catheline S, Callot T. Proceedings of the IEEE ultrasonics symposium; 2011 p. 1160.
26. Gallot T, Catheline S, Roux P, Brum J, Benech N, Negreira C. IEEE Trans Ultrason Ferroelectr Freq Control. 2002;58:1122.